Available online at www.sciencedirect.com
ScienceDirect
Journal of Nuclear Materials 374 (2008) 339–343
journal of nuclear materials
www.elsevier.com/locate/jnucmat

EXAFS and XANES studies of americium dioxide with fluorite structure

Tsuyoshi Nishi [a,*], Masami Nakada [a], Akinori Itoh [a], Chikashi Suzuki [b], Masaru Hirata [a], Mitsuo Akabori [a]

[a] Nuclear Science and Engineering Directorate, Japan Atomic Energy Agency, Tokai-mura, Ibaraki 319-1195, Japan
[b] Advanced Nuclear System Research and Development Directorate, Japan Atomic Energy Agency, Oarai-machi, Ibaraki 311-1393, Japan

Received 8 June 2007; accepted 2 September 2007

Abstract

EXAFS and XANES analyses were applied in a study of americium dioxide (AmO_2) with fluorite structure. EXAFS result for Am-L_{III} absorption edge of AmO_2 was in good agreement with the long-ranged structural data from X-ray diffraction analysis. In order to characterize XANES in aspect of the electronic structure, the theoretical assignment for the AmO_2 was performed with the relativistic DV-Xα molecular orbital method. The calculated XANES spectrum well reproduced the experimental spectrum. From this theoretical assignment, it was found that the peaks of the XANES spectrum were created due to the specific hybridization of orbital components.

PACS: 33.20.Rm (X-ray spectra)

1. Introduction

Minor actinides (MAs: Np, Am and Cm) are accumulated in an irradiated nuclear fuels. To reduce the potential long-term hazard of radioactive wastes, transmutation of MAs is considered to be an important option for the future nuclear fuel cycle. For these backgrounds, various types of fuels containing MAs have been investigated for fast reactors (FRs) or transmutation systems such as accelerator driven systems (ADS). Among these fuels, mixed oxide containing MAs (MA-MOX) is a promising candidate fuel for the transmutation of MA in FRs [1,2]. Therefore, the local and electronic structures around Am atom in the oxide fuels are indispensable information because the valence state of Am strongly affects the oxygen potentials and thermal properties of MA-MOX fuels.

The X-ray absorption fine structure (XAFS) technique including the extended X-ray absorption fine structure (EXAFS) and the X-ray absorption near-edge structure (XANES) is an excellent method for examining the local and electronic structures surrounding an actinide atom in oxide fuels [3–7]. In particular, XANES gives the information on the electronic structures of unoccupied molecular orbital. Martin and co-workers applied the XAFS technique to investigate the local structure of actinide atoms and simulated fission products in UO_2 and other oxide fuels [5–7]. They demonstrated the efficacy of the EXAFS to study the local structure of these minor constituents in the fuel matrixes. However, despite of the importance of structural and electronic information of Am in the fuel matrixes, the XAFS studies of americium are only limited to several compounds and complexes, such as $Pb_2Sr_2AmCu_3O_8$ [8] and $Am(OH)_3$ [9].

In this paper, the local and electronic structures around Am atom in AmO_2 are characterized by transmission XAFS measurement with the synchrotron radiation source and the XANES spectra were theoretically assigned by using the relativistic DV-Xα molecular orbital method.

* Corresponding author. Tel.: +81 29 282 5431; fax: +81 29 282 5922.
E-mail address: nishi.tsuyoshi@jaea.go.jp (T. Nishi).

0022-3115/$ - see front matter © 2007 Elsevier B.V. All rights reserved.
doi:10.1016/j.jnucmat.2007.09.001

2. Experimental

2.1. Sample preparation

The stoichiometric AmO_2 powder for the XAFS measurements was prepared by heating the as-received $^{243}AmO_2$ powder at 1173 K for 2 h and then 1073 K for 2 h both in air atmosphere. The purity of the AmO_2 powder was about 99.7% for nonradioactive impurities [10]. The sample was also examined by powder X-ray diffraction analysis with Cu Kα radiation to identify the phases and to determine the lattice parameter. The X-ray diffraction pattern is shown in Fig. 1, where ZrN powder is used as an internal standard. The X-ray diffraction analysis revealed that the sample was composed of fcc phase with the lattice parameter of 0.5379 nm.

The AmO_2 and graphite powders were stirred to combine by an agate mortar and then pressed into a disk. The diameter of the disk was 6 mm. The weight of AmO_2 was 5.6 mg, which was corresponding to 37 MBq, and that of graphite was 41 mg. The optimum sample thickness of AmO_2 for transmission XAFS measurement was determined by the equation; $\Delta\mu t = 1$, where $\Delta\mu$ is the absorption edge jump of Am and t is the optimum sample thickness for transmission XAFS measurement. The optimum sample thickness, which was estimated from the $\Delta\mu$ of Am [11], was found from calculation to be 13.5 μm. The disk was doubly sealed in two polyethylene terephthalate (PET) containers by the use of epoxy resin (stycast 1266).

2.2. XAFS measurements

The XAFS measurements at Am L_{III}-edge of AmO_2 were performed in transmission mode at the hard X-ray station BL-27 of the Photon Factory, High Energy Accelerator Research Organization (KEK), operating at energy of 3.0 GeV. The radiation was monochromatized by a double-crystal Si(1 1 1) monochromator. The intensities of incident and transmitted beams were monitored by ionization chamber in Ar/N_2 gas and Ar gas flow, respectively. The EXAFS and XANES spectra were recorded at room temperature. Energy calibration of EXAFS and XANES spectra were achieved using the Zr foil (K-edge: 17.998 keV [12]) references positioned in front of the AmO_2 sample. The EXAFS and differentiated EXAFS spectra of Zr foil and AmO_2 are shown in Fig. 2. The energy of white-line peak for AmO_2 was 18.522 keV.

2.3. Analyses of EXAFS and XANES spectra

The EXAFS spectrum was analyzed in the conventional way with the computer program WinXAS version 3.1 [13]. The interatomic distances and coordination numbers of AmO_2 were determined from fitting the inverse Fourier transform of the isolated contribution of interest shells on the R-space distributions to the EXAFS equation, where the EXAFS analysis was based on the back-scattering amplitudes and phase shifts calculated by FEFF 7 code [14] theoretical calculation using the AmO_2 crystallographic data from the XRD analysis.

The XANES spectrum was analyzed by the relativistic DV-Xα molecular orbital method [15,16]. The model clusters $[AmO_8]^{12-}$ with O_h symmetry was used for the calculation of infinite size solids. Bond length was 0.2329 nm which was taken from the first correlation of Am–O pair. The cluster was embedded in an external field composed of point charge of +4 and −2 at the lattice sites of Am and O, respectively, which produced a Madelung potential. The basis sets were Am 1s-11p and O 1s-7p. The number of random sampling points in the DV-Xα calculation was 18 000, namely, 2000 points per atom. Slater's exchange parameter (α) was fixed at 0.7 for all the atoms in the cluster.

3. Results and discussion

3.1. EXAFS analysis of AmO_2

Fig. 3 shows the EXAFS spectrum of Am-L_{III} absorption edge of AmO_2. The resultant k^3-weighted EXAFS

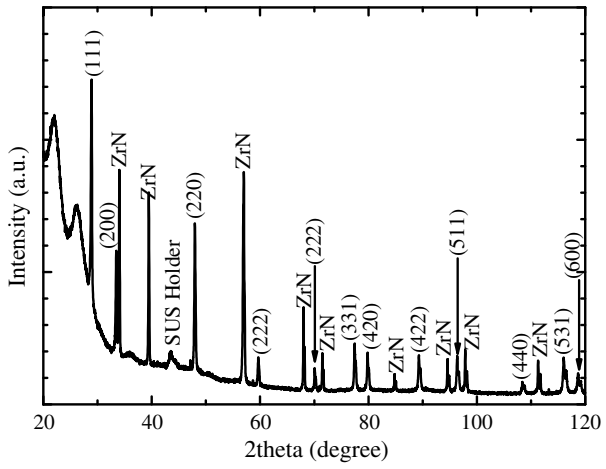

Fig. 1. X-ray diffraction pattern of AmO_2 together with ZrN powder as an internal standard.

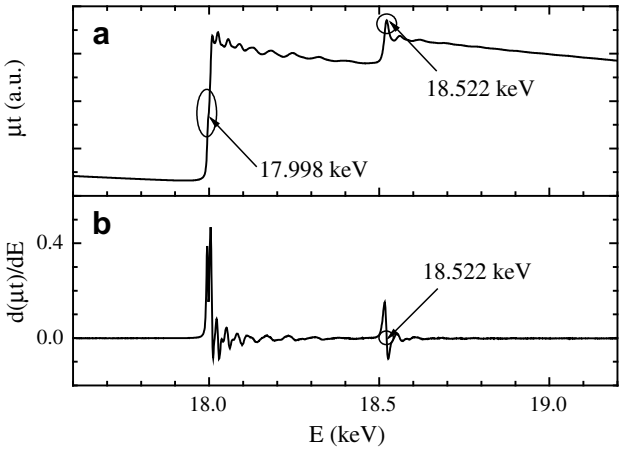

Fig. 2. EXAFS spectra of Zr foil (K-edge) and AmO_2 (L_{III}-edge): (a) EXAFS spectrum and (b) differentiated EXAFS spectrum.

oscillation is given in Fig. 4, where the broken line corresponds to the calculated one to fit the experimental data. The structural parameters of four coordination shells in near neighbors are summarized in Table 1. As shown in Fig. 4, it was found that experimental EXAFS oscillation was in good agreement with the calculated one. In addition, the Fourier transform of k^3-weighted EXAFS oscillation is shown in Fig. 5, where the peaks are not expected to correspond exactly to the true neighboring atomic distances, because the Fourier transform is produced without consideration of the absorber and scattered phase shifts for the backscattering atoms. As shown in Fig. 5 and Table 1, the first peak ($r = 0.2318$ nm) and second peak ($r = 0.3803$ nm) on the R-space distribution are attributed to a shell of nearest neighbor O and Am atoms, respectively. The third peak ($r = 0.4461$ nm) and fourth peak ($r = 0.5401$ nm) are due to a shell of second-nearest O and Am atoms, respectively.

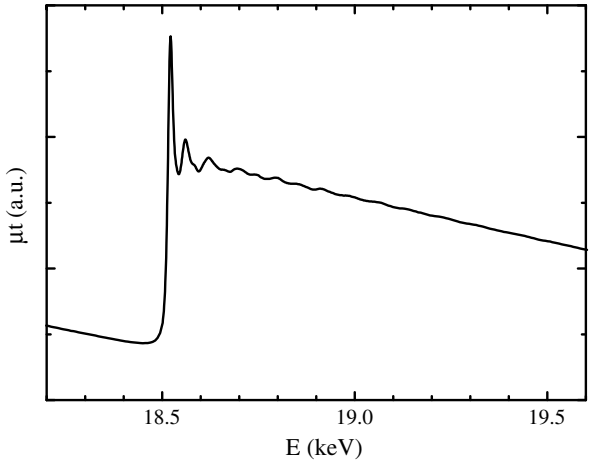

Fig. 3. Experimental EXAFS spectrum of Am L_{III} absorption edge for AmO_2.

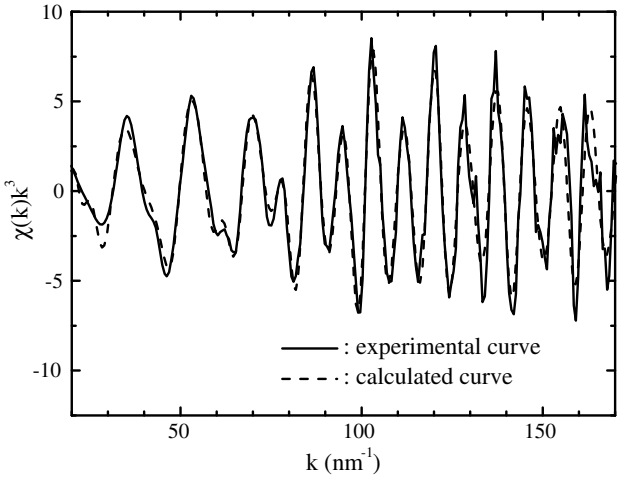

Fig. 4. k^3-weighted EXAFS oscillation of Am-L_{III} edge for AmO_2.

Table 1
The structural parameters of four coordination shells in near neighbors

Shell	Experimental results from EXAFS analysis			Experimental results from X-ray diffraction analysis	
	r (nm)	N	$\Delta\sigma^2$ (nm^2)	r (nm)	N
Am–O	0.2318	8.1	6.8	0.2329	8
Am–Am	0.3803	11.7	4.7	0.3804	12
Am–O	0.4461	24.5	9.7	0.4460	24
Am–Am	0.5401	5.8	5.7	0.5379	6

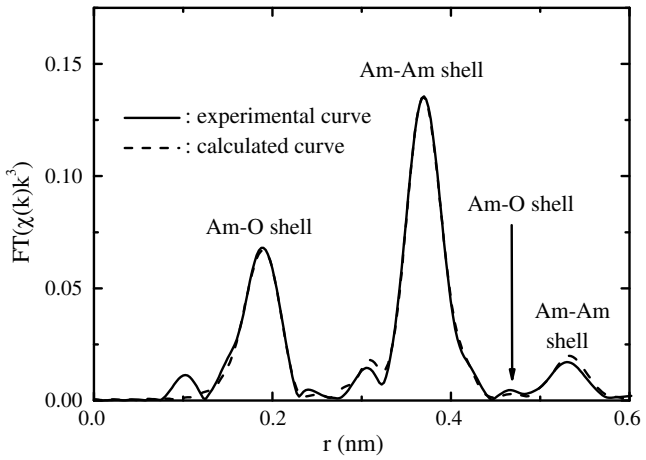

Fig. 5. R-space distribution of Am-L_{III} edge for AmO_2.

3.2. Electronic structure of AmO_2 related with XANES spectrum

The experimental XANES spectrum of Am-L_{III} edge for AmO_2 is shown in Fig. 6(a). It could be expressed that there were two peaks (peak A, B) in this spectrum. Additionally, the tail peak A′ was observed beside the peak A.

The calculated XANES spectrum of AmO_2 and the transition probability from molecular orbital (MO) mainly composed of Am $2p_{3/2}$ are shown in Fig. 6(b). The peak width (FWHM) of each Gaussian curve was set to 6.0 eV for the calculated spectrum. The two peaks (peak A, B) and the tail peak A′ were well reproduced. As shown in Fig. 6(b), the white-line peak A was attributed to two MO ($9\gamma_{7g}$ and $13–16\gamma_{8g}$). The tail peak A′ was attributed to $22\gamma_{8g}$. The peak B was attributed to $28\gamma_{8g}$, $18–19\gamma_{7g}$ and $33–34\gamma_{8g}$.

The main atomic orbital components of the unoccupied MO are shown in Table 2. $13\gamma_{8g}$ originated from the hybridization between Am d and O d components, and Am d component was made up of a majority of $13\gamma_{8g}$. In $9\gamma_{7g}$, Am d, O p, and O d components could be regarded as similar. In $16\gamma_{8g}$, Am d component was primary hybridized with O p, but O d component could not be ignored. From these results, the white-line peak A was created due to the hybridization between Am d and O p and d components.

In $22\gamma_{8g}$, Am d component was hybridized primary with O d, which was made up of a majority of $22\gamma_{8g}$, and

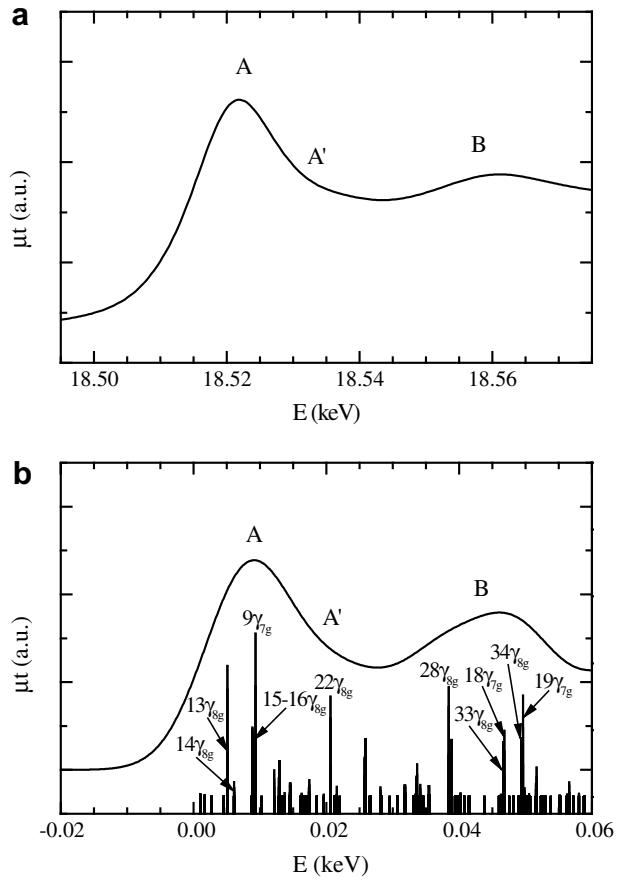

Fig. 6. XANES spectra of Am L_{III} absorption edge for AmO_2: (a) Experimental spectrum and (b) calculated spectrum together with the transition probability from the MO mainly composed of Am $2p_{3/2}$.

minority of O f. Therefore, the tail peak A′ was created primary due to the hybridization between Am d and O d components, but O f component could not be ignored.

In $28\gamma_{8g}$, Am d component was hybridized with and O f, which was made up of a majority of $28\gamma_{8g}$. In 18–$19\gamma_{7g}$ and 33–$34\gamma_{8g}$, Am d and O s, p, d, and f components were 0.06–0.10, 0.09–0.18, 0.16–0.21, 0.24–0.27 and 0.28–0.39, which were similar and no specific component was made up of a majority of each of 18–$19\gamma_{7g}$ and 33–$34\gamma_{8g}$. Therefore, the peak B was divided into the two components.

In these results, it is expected that the theoretical assignment of the XANES spectra for actinide oxides such as AmO_2 is very useful for the development of MA-MOX fuel for the future nuclear fuel cycle.

4. Conclusions

The local and electronic structures around Am atoms in AmO_2 are characterized by transmission XAFS measurement with the synchrotron radiation source using the conventional way of EXAFS analysis and the MO calculation of XANES analysis. The conclusions were as follows:

Table 2
The main atomic orbital components of the unoccupied MO of the transition probability from the MO mainly composed of Am $2p_{3/2}$

MO	Energy (eV)[a]	Am d	O s	O p	O d	O f
$13\gamma_{8g}$	5.11	0.668	0.008	0.019	0.283	0.022
$14\gamma_{8g}$	6.07	0.044	0.542	0.322	0.065	0.027
$15\gamma_{8g}$	8.84	0.299	0.029	0.347	0.290	0.035
$16\gamma_{8g}$	8.92	0.180	0.019	0.568	0.202	0.030
$9\gamma_{7g}$	9.32	0.446	0.071	0.130	0.314	0.039
$22\gamma_{8g}$	20.63	0.198	0.000	0.044	0.605	0.152
$28\gamma_{8g}$	38.45	0.177	0.006	0.043	0.026	0.748
$33\gamma_{8g}$	46.65	0.097	0.098	0.180	0.262	0.363
$18\gamma_{7g}$	46.82	0.085	0.118	0.163	0.249	0.385
$34\gamma_{8g}$	49.38	0.066	0.179	0.160	0.254	0.343
$19\gamma_{7g}$	49.63	0.080	0.178	0.207	0.254	0.280

[a] The energy of the LUMO is set to zero.

The structural parameters obtained from EXAFS analysis of AmO_2 were in good agreement with those obtained from X-ray diffraction analysis.

The calculated XANES spectrum well reproduced the experimental XANES spectrum and assigned theoretically. From this theoretical assignment, it was found that the peaks of the XANES spectrum were created due to the specific hybridization of orbital components.

Acknowledgement

The authors are grateful to Professor K. Kobayashi, the Institute of Materials Structure Science of High Energy Accelerator Research Organization (KEK), Drs Y. Okamoto, Y. Arai and K. Minato, JAEA for his helpful advice, and Mr M. Kamoshida, Chiyoda Maintenance Corporation for their kind supports. The authors are also grateful to Professor K. Ogasawara and Dr H. Yoshida of Kwansei Gakuin University for providing the computer program for the XANES analysis.

References

[1] H. Yoshimochi, M. Nemoto, K. Mondo, S. Koyama, T. Namekawa, J. Nucl. Sci. Tech. 41 (2004) 850.
[2] K. Morimoto, M. Kato, H. Uno, A. Hanari, T. Tamura, H. Sugata, T. Sunaoshi, S. Kono, J. Phys. Chem. Solid. 66 (2005) 634.
[3] M.A. Denecke, Coord. Chem. Rev. 250 (2006) 730.
[4] K.E. Roberts, T.J. Wolery, C.E. Atkins-Duffin, T.G. Prussin, P.G. Allen, J.J. Bucher, D.K. Shuh, R.J. Finch, S.G. Prussin, Radiochim. Acta 91 (2003) 87.
[5] P. Martin, M. Ripert, G. Carlot, P. Parent, C. Laffon, J. Nucl. Mater. 320 (2003) 138.
[6] P. Martin, M. Ripert, T. Petit, T. Reich, C. Henning, F. D′Acapito, J.L. Hazemann, O. Proux, J. Nucl. Mater. 320 (2003) 138.
[7] P. Martin, M. Ripert, G. Carlot, P. Parent, C. Laffon, J. Nucl. Mater. 326 (2003) 132.
[8] L. Soderholm, C. Williams, S. Skanthakumar, M.R. Antonio, S. Conradson, Z. Phys. B 101 (1996) 539.
[9] D. Meyer, S. Fouchard, E. Simoni, C. DenAuwer, Radiochim. Acta 90 (2002) 253.
[10] T. Nishi, M. Takano, A. Itoh, M. Akabori, K. Minato, M. Kizaki, J. Nucl. Mater. 355 (2006) 114.

[11] Y. Waseda, Anomalous X-ray Scattering for Materials Characterization, Springer, Germany, 2002, pp. 205–207.
[12] J.A. Bearden, A.F. Burr, Rev. Mod. Phys. 39 (1967) 125.
[13] T. Ressler, J. Synch. Rad. 5 (1998) 118.
[14] A.L. Ankudinov, J.J. Rehr, Phys. Rev. B 56 (1997) R1712.
[15] A. Rosén, D.E. Ellis, H. Adachi, F.W. Averii, J. Chem. Phys. 65 (1976) 3629.
[16] H. Nakamatsu, Chem. Phys. 200 (1995) 49.